Bifunctional silica nanoparticles for the exploration of biofilms of *Pseudomonas aeruginosa*

L. Mauline[a], M. Gressier[a], C. Roques[b], P. Hammer[c], S.J.L. Ribeiro[d], J.M.A. Caiut[e] and M.-J. Menu[a]*

[a]*Centre Interuniversitaire de Recherche et de l'Ingénierie des Matériaux, UMR-CNRS 5085, Université Paul Sabatier, Toulouse cedex 9, France;* [b]*Laboratoire de Génie Chimique, UMR-CNRS 5503, Université Paul Sabatier, Toulouse cedex 9, France;* [c]*Laboratório de Espectroscopia de Fotoelétrons, LEFE, Institute of Chemistry, São Paulo State University, UNESP, Araraquara – SP, Brazil;* [d]*Institute of Chemistry, São Paulo State University, UNESP, Araraquara – SP, Brazil;* [e]*Department of Chemistry, FFLCRP, University of São Paulo, Ribeirão Preto – SP, Brazil*

Luminescent silica nanoparticles are frequently employed for biotechnology applications mainly because of their easy functionalization, photo-stability, and biocompatibility. Bifunctional silica nanoparticles (BSNPs) are described here as new efficient tools for investigating complex biological systems such as biofilms. Photoluminescence is brought about by the incorporation of a silylated ruthenium(II) complex. The surface properties of the silica particles were designed by reaction with amino-organosilanes, quaternary ammonium-organosilanes, carboxylate-organosilanes and hexamethyldisilazane. BSNPs were characterized extensively by DRIFT, ^{13}C and ^{29}Si solid state NMR, XPS, and photoluminescence. Zeta potential and contact angle measurements exhibited various surface properties (hydrophilic/hydrophobic balance and electric charge) according to the functional groups. Confocal laser scanning microscopy (CLSM) measurements showed that the spatial distribution of these nanoparticles inside a biofilm of *Pseudomonas aeruginosa* PAO1 depends more on their hydrophilic/hydrophobic characteristics than on their size. CLSM observations using two nanosized particles (25 and 68 nm) suggest that narrow diffusion paths exist through the extracellular polymeric substances matrix.

Keywords: bifunctional silica nanoparticles; photoluminescence; surface modification; *P. aeruginosa* (PAO1) biofilms

Introduction

A biofilm can be described as a community of microorganisms adhering to a surface and generally entrapped in a self-produced matrix of extracellular polymeric substances (EPS) (Costerton et al. 1995). The formation of biofilms is a widespread phenomenon with a major economic impact in industrial (Little et al. 2008; Lau et al. 2009), medical (Hall-Stoodley & Stoodley 2005; Huq et al. 2008), and environmental fields (Singh et al. 2006; Wahl et al. 2012). In the medical field, bacterial biofilms play an important role in nosocomial infections, around 65% of which are due to the contamination of medical devices (eg implants or catheters). Life-threatening infections caused by biofilms of *Pseudomonas aeruginos*a in patients with cystic fibrosis is also a well-known example (Doggett et al. 1966).

A distinctive feature of biofilms is their high resistance towards antibiotic and disinfectant agents, which is greater than that of planktonic cells (Brooun et al. 2000; Mah & O'Toole 2001; White & McDermott 2001). Besides the modification of genomic expression leading to cellular phenotypic resistance (Brooun et al. 2000), the resistance exhibited by a biofilm can be linked to its complex 3D structure which includes channels, microcolonies, and mushroom-like protrusions (Lawrence et al. 1991; Mah & O'Toole 2001) and to the presence of a matrix of EPS composed of polysaccharides, proteins, and DNA (Wingender et al. 1999; Mah & O'Toole 2001). Therefore, understanding the role of the 3D structure and of the EPS would provide invaluable information into the control and/or the eradication of biofilms.

The development of imaging techniques, in particular fluorescence microscopy coupled with functionalized nanoprobes, allows *in situ* investigations of the 3D structure of biofilms with submicron resolution. For nearly two decades, luminescent latex nanoparticles combined with confocal laser scanning microscopy (CLSM) have been intensively employed for the investigation of mass transport, particle spatial distribution, and diffusion inside biofilms. De Beer, Stoodley, Roe et al. (1994), de Beer, Stoodley, Lewandowski et al. (1994) and Stoodley et al. (1994) clearly showed the presence of convective flows in channels within the biofilm using fluorescent latex particles of 1 μm and 0.28 μm diameters, respectively. Drury, Characklis, et al. (1993), Drury, Stewart, et al. (1993) and Okabe et al. (1997) described the penetration of luminescent micrometric latex particles in both biofilms of *P. aeruginosa* and a mixed biofilm. In addition to this, evidence of the uptake and release of particles has been shown due to the heterogeneities of mixed

*Corresponding author. Email: menu@chimie.ups-tlse.fr

biofilms. More recently, Tripathi et al. (2012) examined the transport behavior of luminescent latex particles in sand coated with a biofilm of *P. aeruginosa*. The effect of particle size was investigated, notably by using nano-sized (20 nm) sulfate-functionalized latex particles. Fluorescence correlation spectroscopy associated with confocal microscopy allowed the diffusion of luminescent latex particles inside biofilms to be investigated with respect to the size and surface charge of the particles. These studies revealed the heterogeneous diffusion of particles inside biofilms (Guiot et al. 2002; Morrow et al. 2010; Habimana et al. 2011; Forier et al. 2012).

Among the variety of available probes such as organic molecules, transition metal complexes or quantum dots (QD), luminescent silica nanoparticles (LSNPs) have been of scientific interest due to their applications in biological and medical fields; such as the rapid and hypersensitive detection of pathogenic bacteria (Zhao et al. 2004; Wang et al. 2010, 2011), cancer cell detection (Santra et al. 2001; Herr et al. 2006), and cell imaging (Voisin et al. 2007; Yang et al. 2008). However, silica nanoparticles are still not widely used in the exploration of biofilms. Hidalgo et al. (2009) investigated the pH microenvironment of biofilms of *Escherichia coli* using pH-sensitive LSNPs with diameters of 70, 30, and 10 nm. Ratiometric core-shell silica nanoparticle sensors were used; Cy5 (insensitive dye) was localized in the silica core while fluorescein (pH sensitive dye) was localized on the silica surface. Using these particles in conjunction with CLSM observations allowed tomographic imaging of the pH.

Compared to latex nanoparticles, silica nanoparticles are amenable to chemical modification because of the presence of silanol groups at the silica surface which allow covalent grafting of different functional groups. Furthermore, appropriate dye can be covalently bound in the core of the silica matrix. For biological applications, covalent anchoring is favored as it prevents dye release, non-specific labeling, and loss of fluorescence signal intensity. Several compounds are described as displaying luminescent properties when covalently incorporated into silica nanoparticles, such as modified QDs (Qian et al. 2010), organic dyes (Yang et al. 2003; Kumar et al. 2008), or transition metal complexes (*d* or *f*) (Jiang et al. 2010). Similar to tris(2,2′-dipyridyl)ruthenium(II) chloride, which is one of the most popular dyes, the synthesis of several silylated ruthenium(II) complexes incorporated into the core or grafted onto the surface of silica nanoparticles has been recently described. These ruthenium(II)–silica nanohybrids display advantages, in particular by exhibiting very interesting photoluminescence properties (Cousinie et al. 2012).

The aim of this study was to evaluate the effect of the surface functionalization of nanoparticles on their spatial distribution in bacterial biofilms. In this work, bifunctional silica nanoparticles (BSNPs) are designed as a luminescent exploration tool. Standard functional groups were chosen to cover the surface of the BSNPs with a functionalized monolayer. Extensive characterization of the synthesized nanoparticles, in both the solid state and in aqueous solutions, was conducted. 3-Aminopropyltriethoxysilane (A), trimethyl(3-trimethoxysilylpropyl)ammonium chloride (B), *N*-(trimethoxysilylpropyl) ethylenediamine triacetic acid trisodium salt (C), and hexamethyldisilazane (D) were chosen as functional groups to amend the surface properties of BSNPs. The molecular structures of the organosilanes and the luminescent ruthenium(II) complex used in this study are detailed in Scheme 1. Interest in these organic functional groups is multiple. Amino- and carboxylate-functions have been widely used for biolabeling thanks to possible bioconjugation with proteins and DNA through peptide bonds (Liu & Han 2005; Shi et al. 2009). The choice of ammonium groups is justified by their ability to change the surface charge of the nanoparticles and because of their reactivity towards bacterial membranes. Hydrophobic functionalization is brought about by the introduction of methyl groups. In this work, BSNPs were prepared by incorporating a silylated ruthenium(II) complex [Ru(bpy)$_2$(bpy-Si)]Cl$_2$ in silica nanoparticles with two particle sizes, and by modifying the surface of LSNPs with four silanes. After checking that LSNPs were non-toxic to *P. aeruginosa*, the effects of surface modification on the penetration and the distribution of BSNPs in biofilms of that species were investigated in detail.

Materials and methods

Synthesis of BSNPs

Synthesis of LSNPs using a quaternary reverse microemulsion

Silica particles were synthesized using the Stöber method in reverse microemulsion. Luminescent characteristics were obtained by incorporating the silylated [Ru(bpy)$_2$(bpy-Si)]Cl$_2$ dye. Cyclohexane (60 cm^3, 555 mmol), *n*-hexanol (14.4 cm^3, 114 mmol), and triton X-100 (14.2 cm^3, 23 mmol) were mixed and shaken vigorously. The complex [Ru(bpy)$_2$(bpy-Si)]Cl$_2$ (50 mg, 0.05 mmol) was then dissolved in ultrapure water (4 cm^3, 222 mmol) and added to the mixture. A clear and stable reverse microemulsion was obtained after stirring for 15 min. TEOS (0.80 cm^3, 3.58 mmol) and drops of aqueous ammonia (0.48 cm^3, 8 mmol) were then introduced at intervals of 15 min. The microemulsion was stirred for 24 h and then broken by adding acetone (150 cm^3). LSNPs were recuperated by centrifugation and several subsequent washing procedures were performed with water, ethanol, and diethyl ether in order to remove surfactants and excess free dye. The isolated powder 130 mg (95%) was dried under vacuum for 2 h.

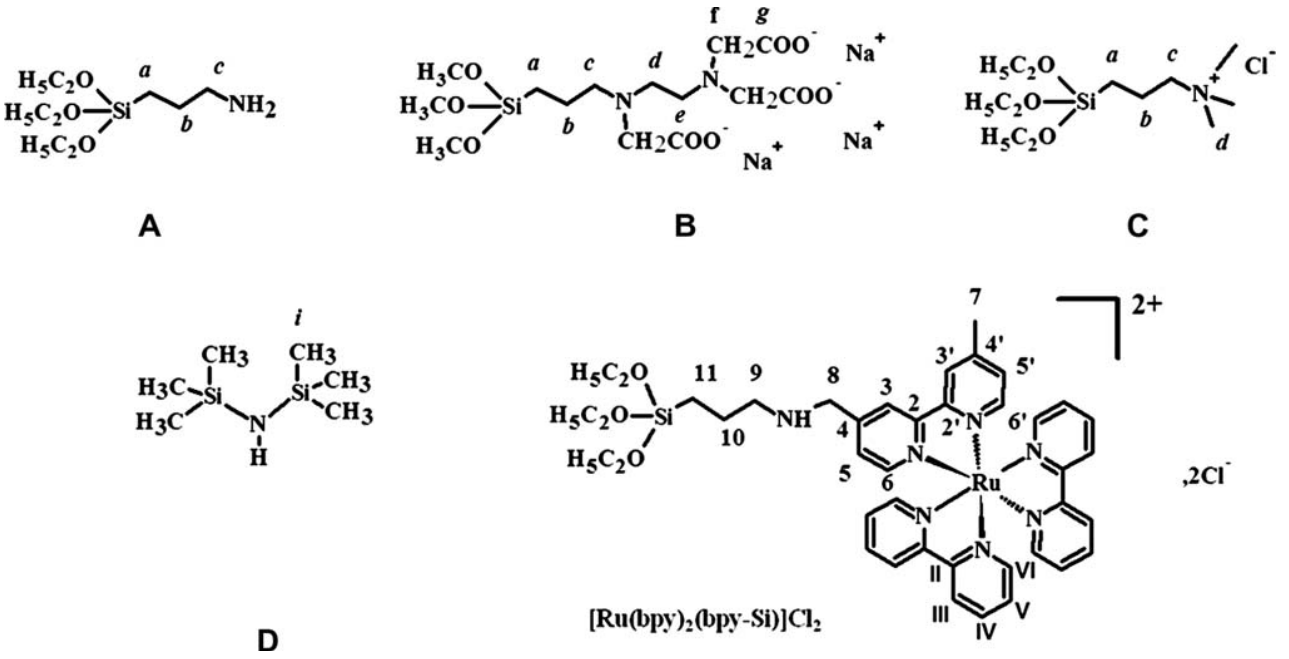

Scheme 1. Molecular structure of the organosilanes and the ruthenium complex $[Ru(bpy)_2(bpy\text{-}Si)]Cl_2$ used to obtain BSNPs. A = 3-Aminopropyltriethoxysilane, B = trimethyl(3-trimethoxysilylpropyl)ammonium chloride, C = *N*-(trimethoxysilylpropyl)ethylenediamine triacetic acid trisodium salt, D = hexamethyldisilazane.

Synthesis of LSNPs using a ternary reverse microemulsion

Cyclohexane (60 cm^3, 555 mmol) and Igepal CO 520 (3 cm^3, 6 mmol) were shaken vigorously. The complex $[Ru(bpy)_2(bpy\text{-}Si)]Cl_2$ (13 mg, 0.01 mmol) was then dissolved in ultrapure water (0.54 cm^3, 30 mmol) added to the mixture and stirred for 15 min in order to obtain a clear and stable microemulsion. TEOS (0.48 cm^3, 2 mmol) and aqueous ammonia (0.36 cm^3, 5 mmol) were introduced dropwise at intervals of 15 min. The microemulsion was stirred for 24 h. The post-treatment was the same as for the quaternary reverse microemulsion. The powder isolated (85 mg, 66%) was dried under vacuum for 2 h.

Surface functionalization of LSNPs

LSNPs were activated by mild thermal treatment at 50 °C in a vacuum for 30 min to remove physisorbed water. LSNPs (100 mg) were dispersed in anhydrous acetonitrile (20 cm^3) and different organosilanes bearing functional groups were introduced. Typically, 0.047 cm^3 of A (0.2 mmol), 0.168 cm^3 of B (0.2 mmol), 0.168 cm^3 of C (0.2 mmol), or 0.042 cm^3 of D (0.2 mmol) were used. The mixture was allowed to reflux for 24 h. BSNPs were purified by cycles of centrifugation, washed with ethanol and diethyl ether and then dried under vacuum for 2 h.

BSNPs are denoted *Ru@Si-X* where *Ru@Si* represents LSNPs and X = A, B, C, or D, the grafted organosilanes as indicated above.

Chemical characterization of BSNPs

^{29}Si and ^{13}C solid-state NMR spectroscopy

^{13}C and ^{29}Si solid-state NMR spectra were recorded on Bruker Avance 400WB equipment using dipolar decoupling in combination with cross-polarization (CP) and magic angle spinning (MAS) (100.356 and 79.391 MHz for ^{13}C and ^{29}Si, respectively).

Photoluminescence

Photoluminescence excitation and emission spectra of BSNPs were recorded at room temperature with a Jobin Yvon, Fluorolog-3 spectrophotometer model FL3-22.

X-ray photoelectron spectroscopy

X-ray photoelectron spectroscopy (XPS) measurements were carried out at a pressure of $<10^{-6}$ Pa using a commercial spectrometer (UNI-SPECS UHV). The Mg Kα line was used ($h\nu = 1253.6$ eV) and the analyzer pass energy was set at 10 eV. The inelastic background of the C 1s, O 1s, N 1s, Si 2p, and Ru 3d electron core-level spectra was subtracted using Shirley's method. The composition of the near-surface region was determined

with an accuracy of 10% from the ratio of the relative peak areas corrected by Scofield's sensitivity factors of the corresponding elements.

Transmission electron microscopy

Transmission electron microscopy (TEM) analyses were carried out on a JEOL 2010 (200 kV). A drop of sol was diluted in ethanol. A carbon-coated grid was dipped in the solution and allowed to air-dry at room temperature.

Hydrodynamic diameter and zeta potential of BSNPs

Zeta potential (ζ) and dynamic light scattering measurements were carried out on a Malvern nanosizer ZS90 equipped with a red laser (633 nm). The hydrodynamic diameter was determined by DLA measurements.

Hydrophilic/hydrophobic balance of BSNPs

Contact angle measurements were made on pellets prepared from the BSNPs. Using a motor driven syringe, a 4×10^{-3} cm^3 drop of water was released onto the pellets, and contact angle was recorded using a CDD camera.

Preparation of* P. aeruginosa *PAO1 biofilms and labeling with BSNPs

Biofilms of *P. aeruginosa* PAO1 were grown for three days under pseudo-static conditions in modified biofilm broth (MBB) to obtain a structured biofilm, rich in EPS (Figure S3, Supplementary information) [Supplementary material is available *via* a multimedia link on the online article webpage.]. These conditions formally optimized by Khalilzadeh et al. (2010), favor the multiplication of bacteria initially adherent to the microplate rather than the growth of planktonic cells. Bacterial biofilms were grown at 37 °C in 24-well (toxicity evaluation) or 6-well (toxicity evaluation and biofilm penetration) microplates containing 2 or 6 cm^3 of MBB, respectively. After an initial inoculation with a bacterial suspension containing 10^3 CFU cm^{-3} of *P. aeruginosa* PAO1, the medium was renewed after 2, 4, 6, 20, 24, and 48 h. Cells of *P. aeruginosa* PAO1, attached to the well plates, were rinsed gently (x2) with sterilized distilled water (DW; 2 or 6 cm^3), before the addition of fresh media. Biofilms were grown for 3 days. After the period of growth, the wells were rinsed and 2 or 6 cm^3 of an aqueous suspension of BSNPs, at a concentration of 0.5 or 0.05 mg cm^{-3}, were added. Before addition, the aqueous suspension of BSNPs was filtered through Millipore membranes (0.2 µm pore size) in order to sterilize it and filter out large aggregates of BSNPs. Particles were allowed 16 h (or 24 h for toxicity evaluation) to diffuse through the biofilms before observations were made with confocal microscopy.

Toxicity of LSNPs

The toxicity of LSNPs in contact with the biofilms was evaluated by counting CFU (24-well microplates), as well as by bacterial viability staining using LIVE/DEAD® Baclight™ (6-well microplates; Molecular Probe, Invitrogen, France). Particles obtained using ternary and quaternary reverse microemulsions methods were tested, and contact time was fixed for a period of 24 h. After 24 h of contact between the biofilms and LSNPs, two successive rinses with 2 cm^3 of sterilized DW were performed in order to eliminate planktonic bacteria. 1 cm^3 of sterilized DW was then introduced and bacteria were gathered using a sterilized spatula for a period of 1 min. In order to count the biomass of the biofilm of *P. aeruginosa* PAO1, samples were dispersed, serially diluted (10-fold dilutions) and 1 cm^3 of each dilution was placed on a trypticase soy agar plate and incubated for 2 days at 37 °C. The LIVE/DEAD® Baclight™ bacterial viability kit allows the double-labeling of bacteria with SYTO9® (λ_{exc} = 488 nm/λ_{em} = 498–533 nm), which is a DNA-stain, and propidium iodide (PI; λ_{exc} = 543 nm/λ_{em} = 575–700 nm), which is an intercalating nucleic acid dye. PI only stains cells with damaged membranes, whereas SYTO9® stains damaged and intact cells. Consequently, labeled cells appear green when intact and orange or red when damage has occurred to the cell membrane. Six-well microplates were used for CLSM. Because PI emits in the red region, silica nanoparticles were synthesized without the silylated dye $[Ru(bpy)_2(bpy\text{-}Si)]Cl_2$, which also emits in the red region. For both quantification methods, a reference well without LSNPs served as a null control and was used in order to compare the results. Experiments were repeated twice and average values are presented.

Observations with CLSM

Once the MBB medium was removed, a 0.05 mg cm^{-3} aqueous suspension of BSNPs, *Ru@Si*, *Ru@Si-A*, *Ru@Si-B*, *Ru@Si-C,* or *Ru@Si-D*, was introduced to the biofilm and left in contact for 16 h. Immediately prior to observation by CLSM, unbound BSNPs were removed by two rinses with DW. All images of the biofilms (toxicity evaluation and biofilm penetration) were captured and recorded with a Leica SP2 confocal laser scanning system equipped with an upright microscope and different laser sources. All of the experiments were performed at room temperature. In order to observe the biofilms directly, a water-immersion objective was used (40 × 0.8 numerical aperture). Image stacks were recorded in the *z*-direction with an increment of 0.4 µm between focal planes. All the acquisitions were obtained in the sequential mode in order to avoid bleed-through.

The EPS matrix was labeled with the lectin ConA-Alexa Fluor®488 (Molecular Probe, Invitrogen, France). After the removal of the MBB medium, 1 cm^3 of

ConA-Alexa Fluor®488 ($100\,\mu g\,cm^{-3}$ in $NaHCO_3$ solution at 0.1 M) was added to the wells. The microplate was placed in the dark for 20 min. Free ConA-Alexa Fluor®488 was subsequently removed with a micropipette and the wells were washed twice with $2\,cm^3$ of DW prior to being filled with $6\,cm^3$ of DW. Bacteria were labeled with a DNA-stain, SYTO45® (Molecular Probe, Invitrogen, France). A $5 \times 10^{-4}\,cm^3$ volume of SYTO45® (5 mM in DMSO) was added to the wells. ConA-Alexa Fluor®488 was excited with an argon laser (at 10% power output, $\lambda_{exc} = 488$ nm) and the fluorescence was collected within the spectral window 498–533 nm. SYTO45® was excited with an argon laser (at 10% power output, $\lambda_{exc} = 458$ nm) and the fluorescence collected in the 468–488 nm region. Finally, BSNPs were excited with a GreNe laser (at 50% power output, $\lambda_{exc} = 543$ nm) and the fluorescence was collected in the 600–700 nm region. The images recorded were processed with the software Image J version 1.42i developed by Wayne Rasband. Z-project, an Image J plug-in, was used to study the penetration profile of BSNPs through biofilms of *P. aeruginosa* PAO1, by tracing the luminescence intensity as a function of biofilm thickness. A region of interest (ROI) inside the biofilm was defined as a cylinder whose area remained the same in all experiments but whose height depends on the thickness of the biofilm.

Results and discussion

Synthesis and characterizations of BSNPs

Luminescent silica nanoparticles

Obtaining LSNPs was the first stage in preparing the BSNPs. LSNPs were synthesized according to Stöber's method in water-in-oil microemulsion. In order to evaluate the effect of size on the ability of BSNPs to penetrate biofilms, two synthesis methods, which yield particles with varying size distributions, were used; a ternary (cyclohexane/Igepal CO 520/water) microemulsion (Jin et al. 2008) and a quaternary (cyclohexane/hexanol/triton X-100/water) microemulsion (Lian et al. 2004; Cousinie et al. 2012). Figure 1 shows the TEM image of LSNPs prepared with both microemulsions. All nanoparticles appeared spherical and monodisperse in size: their mean diameters were 25 ± 5 nm for the ternary microemulsion (Figure 1I) and 68 ± 2 nm for the quaternary microemulsion (Figure 1II). The average size was determined from ~80 particles.

Different techniques were used to characterize LSNPs (DRIFT and the results of elemental analysis are given in the Supplementary information; Table S1). The incorporation ratio of ruthenium complex (τ_{Ru}) expressed in mmol of complexes g^{-1} silica in LSNPs was determined using the nitrogen content obtained by elemental analysis. For LSNPs resulting from ternary and quaternary microemulsions, τ_{Ru} values were calculated as 0.09 and $0.21\,mmol\,g^{-1}$, respectively. NMR, XPS, DRIFT, and zeta potential analyses were the same irrespective of the size of the LSNPs. The presence of different atoms in the LSNPs was confirmed by XPS analyses. Figure 2 shows the survey spectrum in which Si 2p at 103.5 eV, Si 2s at 154.3 eV, Ru 3d C 1s at 285.0 eV, N 1s at 398.6 eV, Ru 3p at 484.9 eV, and O 1s 532.0 eV photoemission peaks were identified for LSNPs. The assignments are in line with previous data (Moulder et al. 1992), exhibiting the presence of silica and the ruthenium complex.

The chemical integrity of the incorporated complex was confirmed using ^{13}C CP MAS NMR spectroscopy. The signals of the carbon atoms of the ruthenium(II) complex incorporated in the silica matrix appear at 124, 139, 150, and 157 ppm (Figure 3Ia) and were assigned to the carbon atoms of the pyridine ligands, C_{III}–C_V, C_{IV}, C_{VI}, and C_{II}, respectively. The carbon atoms of the propyl chain of the silylated-dye appear with low intensity at 10, 21, and 53 ppm (Cousinie et al. 2012). ^{29}Si CP MAS NMR provided information about the silicon atom environment. The presence of the complex was revealed by a weak T^3 peak at −67 ppm indicating covalent bonding and complete condensation of the alkoxysilyl groups with the silica matrix (Brinker & Scherer 1990; Cousinie et al. 2012). The spectrum of LSNPs (Figure 3IIa) exhibits three characteristic peaks at −92, −101, and −110 ppm assigned to the silanol (Q^2, Q^3) and siloxane (Q^4) groups of the silica matrix, respectively (Maciel & Sindorf 1980; Sindorf & Maciel 1983). The presence of Q^2 and Q^3 peaks, ie silanol groups at the silica surface indicates that surface functionalization is possible after the incorporation of the ruthenium(II) complex.

Figure 4 shows the excitation and emission spectra of LSNPs in aqueous media. In the excitation spectrum, an intense absorption band in the UV region, assigned to ligand-centered $\pi \rightarrow \pi^*$ transitions is observed at 286 nm (Lytle & Hercules 1969). The band observed at 456 nm has been assigned to spin-allowed metal ligand charge transfer (MLCT) $d(Ru) \rightarrow \pi^*$ transitions. In the emission spectrum, a broad band spreading from 610 to 765 nm characteristic of the ruthenium(II) complex is observed.

Bifunctional silica nanoparticles

Surface modification of LSNPs was performed by grafting organosilanes onto the silica particles. The grafting reaction is a nucleophilic substitution (Sutra et al. 1999) between the silanol groups and silicon atoms of the different organosilanes used. The grafting reaction took place in anhydrous acetonitrile and 2 mmol of organosilane g^{-1} silica. These conditions were used for several reasons the most important of which is that by refluxing in anhydrous organic solvents the hydrolysis and

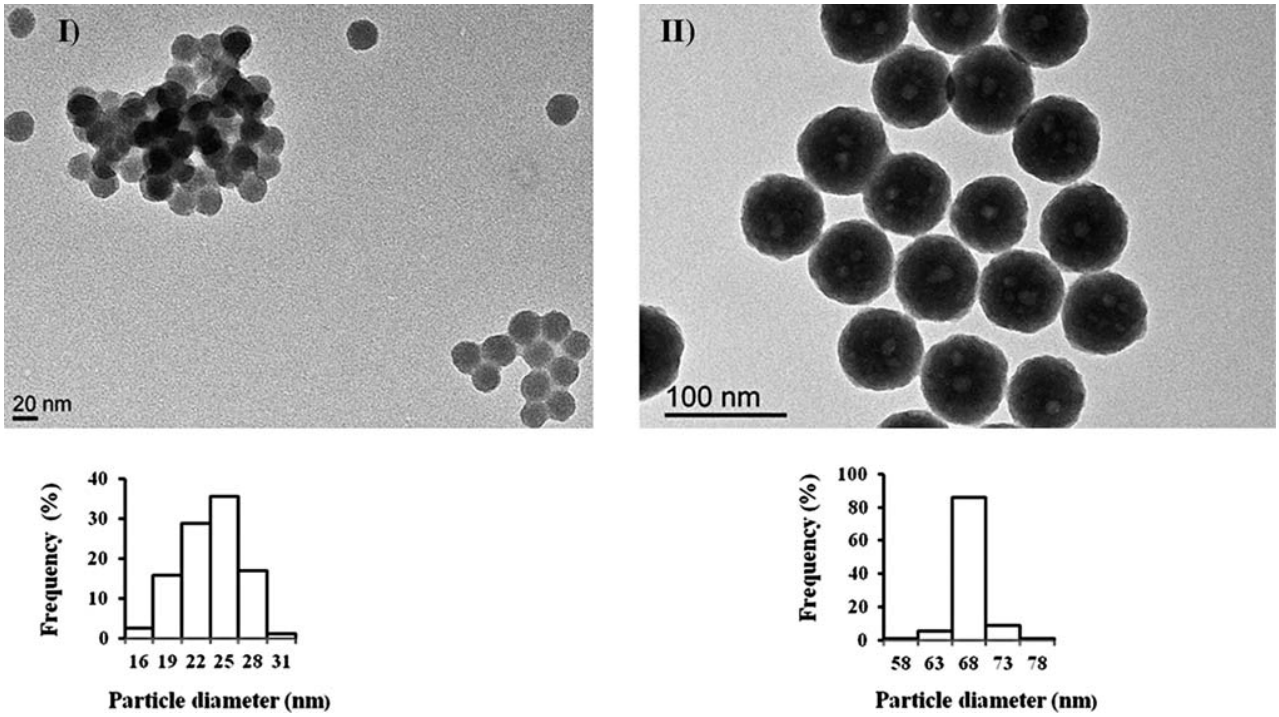

Figure 1. TEM image of *Ru@Si* obtained with ternary microemulsion (I) and *Ru@Si* obtained with quaternary microemulsion (II). The histograms show the particle size distribution as determined by TEM. n=80.

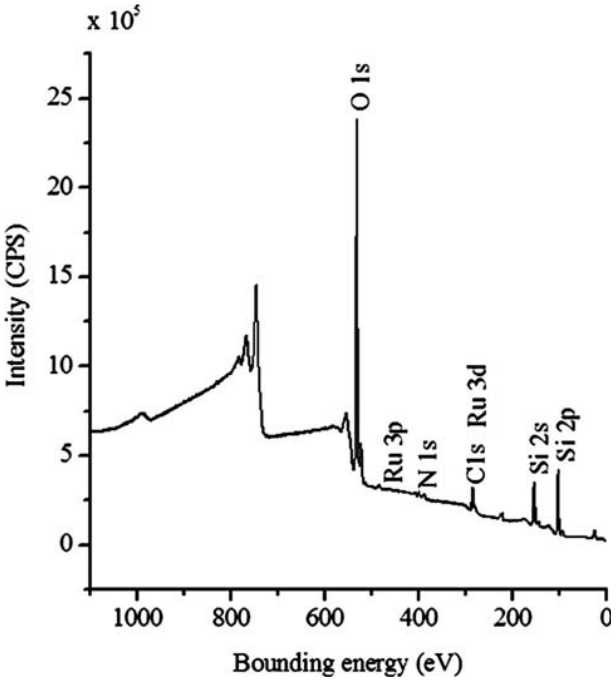

Figure 2. XPS survey spectra of LSNPs.

polymerization of organosilanes is prevented, leading to a monolayer of organosilanes being grafted onto the silica surface. Secondly, organosilanes are more soluble in organic solvents, giving rise to a homogeneous reaction mixture for grafting. Two nanosized LSNPs were functionalized with the four selected organosilanes. These sets of BSNPs were characterized extensively.

The grafting ratios of organosilanes (τ_X) expressed in mmol of grafted organosilanes g^{-1} silica were determined by elemental analysis. The values are reported in Table 1. Based on previous work (Cousinie et al. 2007), a monolayer coverage was ascertained when the grafting ratio was below $1\,\text{mmol}\,g^{-1}$, indicating that materials with controlled surface modifications have been synthesized. This limit value was derived by taking into account the specific surface area of the LSNPs and the average area occupied by one organic molecule.

^{29}Si CP MAS NMR (Figure 3II) is a powerful tool, highlighting the formation of covalent bonds between the organosilanes and the silica matrix in the presence of T type silicon atoms. All spectra were recorded in the same conditions and, in the lower field range, significant increases of the T^3 (-67 ppm) and T^2 (-57 ppm) signals relative to the signal observed for the starting LSNPs were observed. As shown in Figure 3IIb–d, this increase was assigned to the covalent grafting of organosilanes on the silica surface. Spectra of *Ru@Si-D* (Figure 3IIe) exhibit M^1-type grafted silicon atoms at 12 ppm corresponding to $Si(CH_3)_3$ moieties (Sindorf & Maciel 1981). The chemical integrity of the functionalized nanoparticles was confirmed by ^{13}C CP MAS NMR measurements

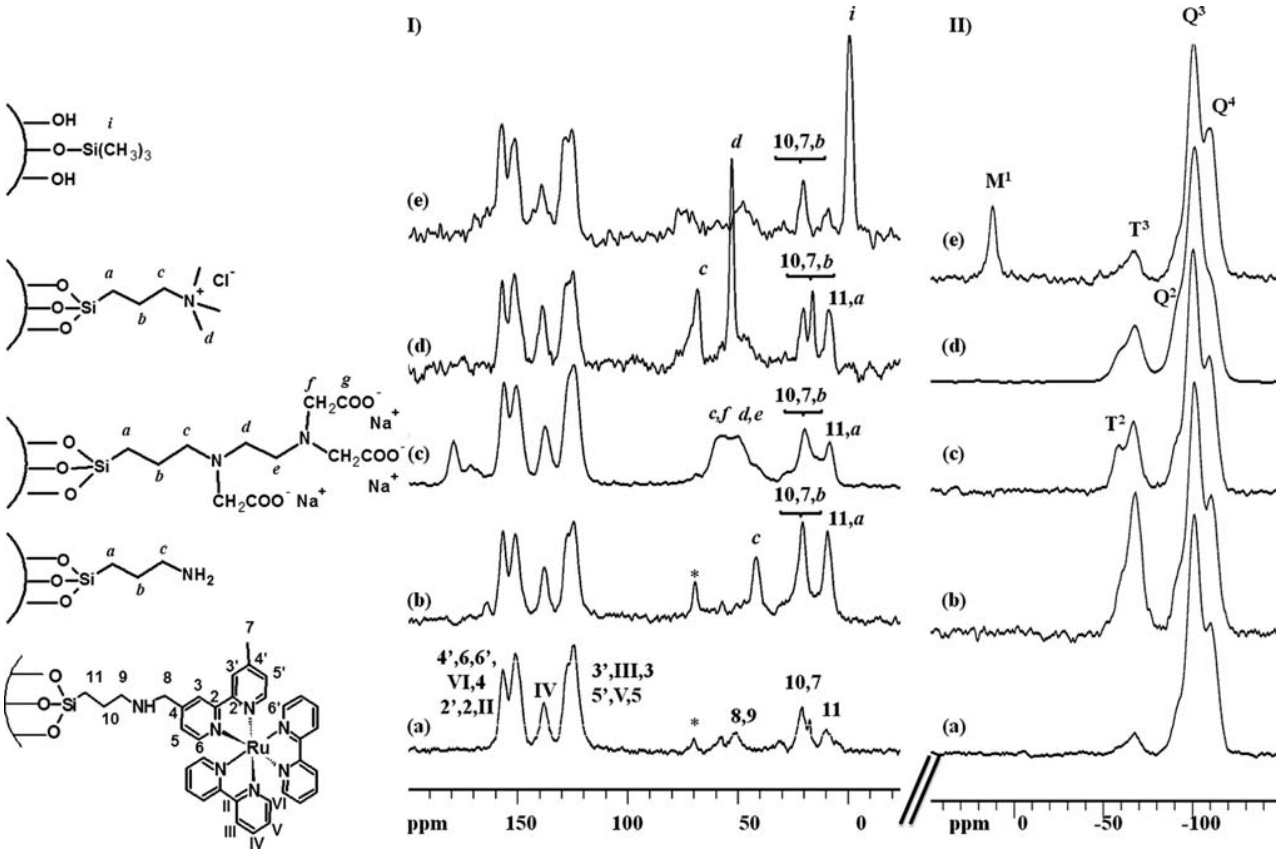

Figure 3. ^{13}C CP MAS NMR spectra (I) and ^{29}Si CP MAS NMR spectra (II) of *Ru@Si* (a), *Ru@Si-A* (b), *Ru@Si-B* (c), *Ru@Si-C* (d), and *Ru@Si-D* (e). The numbering of carbon atoms is given on the left side with Roman figures for the bipyridine ligand; Arabic numerals for the silylated bipyridine ligand and italic lower case letters for the grafted organosilanes.

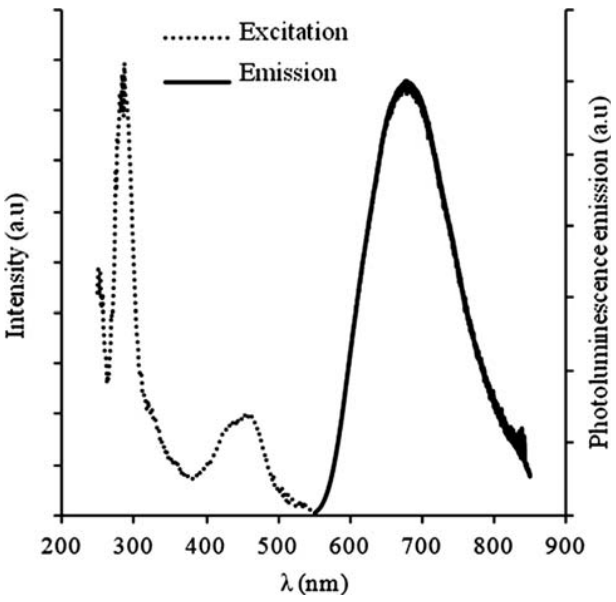

Figure 4. Excitation and emission spectra of LSNPs.

and the assignment of carbon atoms to each functional group is shown in detail in the representation of the carbon atom numbering (Figure 3I). In all spectra, signals in the range 110–160 ppm were assigned to carbon atoms of the dipyridine moiety of the ruthenium complex. In the spectra obtained for BSNPs, more intense peaks can be observed in the high field range corresponding to the carbon atoms of the organosilanes grafted at the surface of the nanoparticles (Figure 3Ib–e).

In regard to *Ru@Si-A* (Figure 3Ib), peaks at 10, 21 and 43 ppm were assigned to the three carbon atoms of the propyl chain of organosilane *A*. The carbon atoms of the carboxylate functions in *Ru@Si-B* are located at 180 ppm (Figure 3Ic) and the carbon atoms of the alkyl chains appear as a broad peak in the range 10–20 ppm and 50–60 ppm. The *Ru@Si-C* spectrum (Figure 3Id) exhibits characteristic signals at 53 and 68 ppm corresponding to $-N^{+}(CH_3)_3$ and $-N^{+}CH_2$ groups, respectively. Trimethylsilyl groups in *Ru@Si-D* appear as an intense signal at 0.3 ppm (Figure 3Ie). These data, exhibiting the presence of functional groups at the surface of the luminescent particles, are in accordance with data collected with the XPS

Table 1. Grafting ratios of BSNPs determined by elementary analysis.

	Grafting ratio (τ_X (mmol g^{-1}))			
Size	*Ru@Si-A*	*Ru@Si-B*	*Ru@Si-C*	*Ru@Si-D*
25 nm	0.93	0.18	1.00	0.31
68 nm	1.00	0.18	0.37	0.56

technique, which allows the characterization of the outermost surface (Supplementary information).

Stable aqueous colloidal sols are required for reliable biological tests. The zeta potential (ζ) is an important physico-chemical parameter since it indicates the degree of repulsion between charged particles in dispersion and thus can be used to evaluate the stability of colloidal suspensions. In accordance with the charge conferred by the organosilanes, the value of the zeta potential varies. The zeta potential of *Ru@Si-A* (0.9 ± 5 mV) is higher than that of *Ru@Si* (-39 ± 5 mV) because the dissociation constant (pKa) of the amino group in organosilane A is ∼10.6 at 298 K thus, in water at pH 6.5, the $-RNH_3^+$ acid form predominates, causing an increase of the zeta potential. On the other hand, the ζ value decreases for *Ru@Si-B* (−47 ± 9 mV) because of the contribution of three negatively charged carboxylates at pH 6.5. As expected, the addition of a quaternary ammonium salt to the silica surface makes the zeta potential largely positive, increasing from −39 mV (*Ru@Si*) to + 43 mV (*Ru@Si-C*). The zeta potential of the LSNPs is very slightly modified when neutral functional groups have been grafted as in *Ru@Si-D* (−32 ± 5 mV). This can be explained by the fact that the number of available SiO^- sites decreased after the grafting reactions leading to a slight increase of zeta potential in comparison with LSNPs. These results confirm the stability of the nanomaterials in solution, with the exception of *Ru@Si-A*, which has a value near 0 mV and thus will tend to aggregate.

In order to understand the nature of the interactions between BSNPs and biofilms of *P. aeruginosa* PAO1, the hydrophilic/hydrophobic nature of the BSNPs was determined with contact angle measurements. The larger the angle (θ) formed by the water drop the greater the hydrophobic character of the material. Figure 5 shows the images of drops formed in contact with the pellets of BSNPs. *Ru@Si*, *Ru@Si-A*, *Ru@Si-B,* and *Ru@Si-C* are hydrophilic with contact angles between 31° and 38°, whereas *Ru@Si-D* appears very hydrophobic with a contact angle >90°.

After organosilane grafting, luminescence properties of the BSNPs were retained, and no changes were observed compared to *Ru@Si*. The spectra of the BSNPs and the LNSPs recorded in the same conditions (concentration 0.5 mg cm^{-3}, excitation wavelength, instrumental parameters) are quantitatively comparable (Figure S2).

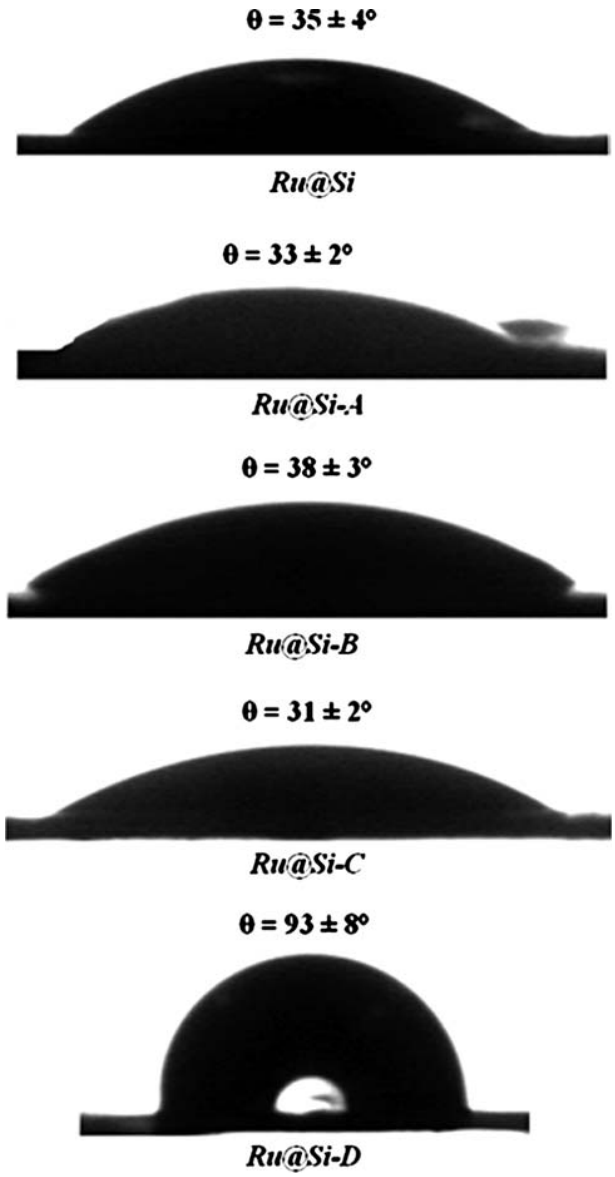

Figure 5. Hydrophilic/hydrophobic balance of BSNPs determined with contact angle measurements. $n = 3$, error bars are SD.

The difference in intensity between the *Ru@Si-D* suspension and the others is due to the fact that at this concentration (10x the concentration used for biofilm exploration), the suspension of hydrophobic nanoparticles is not stable and some aggregates of *Ru@Si-D* particles are observed at the air–water interface. In addition to this and in accordance with the units of the *y*-axis, the intensity of the luminescence displayed by the *Ru@Si-D* suspension remains suitable for observation.

Evaluation of the toxicity of LSNPs

Biocompatibility tests of LSNPs on human (Jin et al. 2008) or animal (Kim et al. 2006) cells have already

been performed. However, no known toxicity study has been performed for the bacteria *P. aeruginosa* and therefore, the toxicity of LSNPs towards biofilms of PAO1 was evaluated. It provided information about the effects of the size and the mass concentration of the particles.

First, bacterial CFU were enumerated in the presence of 68 nm LSNPs with mass concentrations between 0.005 and 5 mg cm^{-3}. Figure 6 shows the log CFU per cm^3 *vs* the concentration of LSNPs, and reveals that at a mass concentration of $\leqslant$0.5 mg cm^{-3} particles have no toxic effects on bacteria. However, at a mass concentration of >0.5 mg cm^{-3}, the number of bacteria decreases by 8%.

To confirm these results, bacterial viability was evaluated in the presence of 25 and 68 nm silica nanoparticles using a LIVE/DEAD® Baclight™ bacterial viability kit with the authorized maximum mass concentration of 0.5 mg cm^{-3}. The LIVE/DEAD® labeling made it possible to evaluate qualitatively the ratio of damaged to viable bacteria. Figure 7 shows the evaluation of the toxicity of LSNPs with diameters of 25 and 68 nm, and a mass concentration of 0.5 mg cm^{-3}. The reference biofilm (Figure 7I), ie that without LSNPs, showed very few damaged cells localized throughout the biofilm, but this tendency was greater inside the biofilm where the bacteria are more numerous. When 25 or 68 nm LSNPs are introduced (Figure 7II–III), the proportion of damaged bacteria was similar to that observed in the reference. These results demonstrate that LSNPs with a size range of 25–68 nm at 0.5 mg cm^{-3} mass concentration were not toxic towards biofilms of *P. aeruginosa* PAO1. These results are in agreement with CFU data and suggest that the maximum concentration of LSNPs should be limited to <0.5 mg cm^{-3} in order to avoid any antibacterial effect.

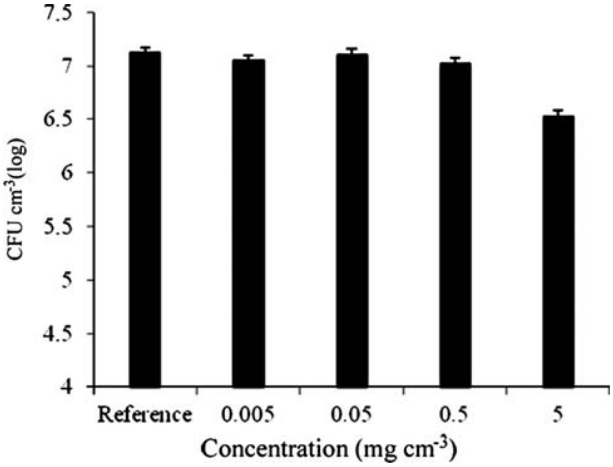

Figure 6. Histogram of bacterial numbers expressed in log CFU cm^{-3} after exposure to 68 nm LNSP for 24 h. $n = 3$, error bars are SE.

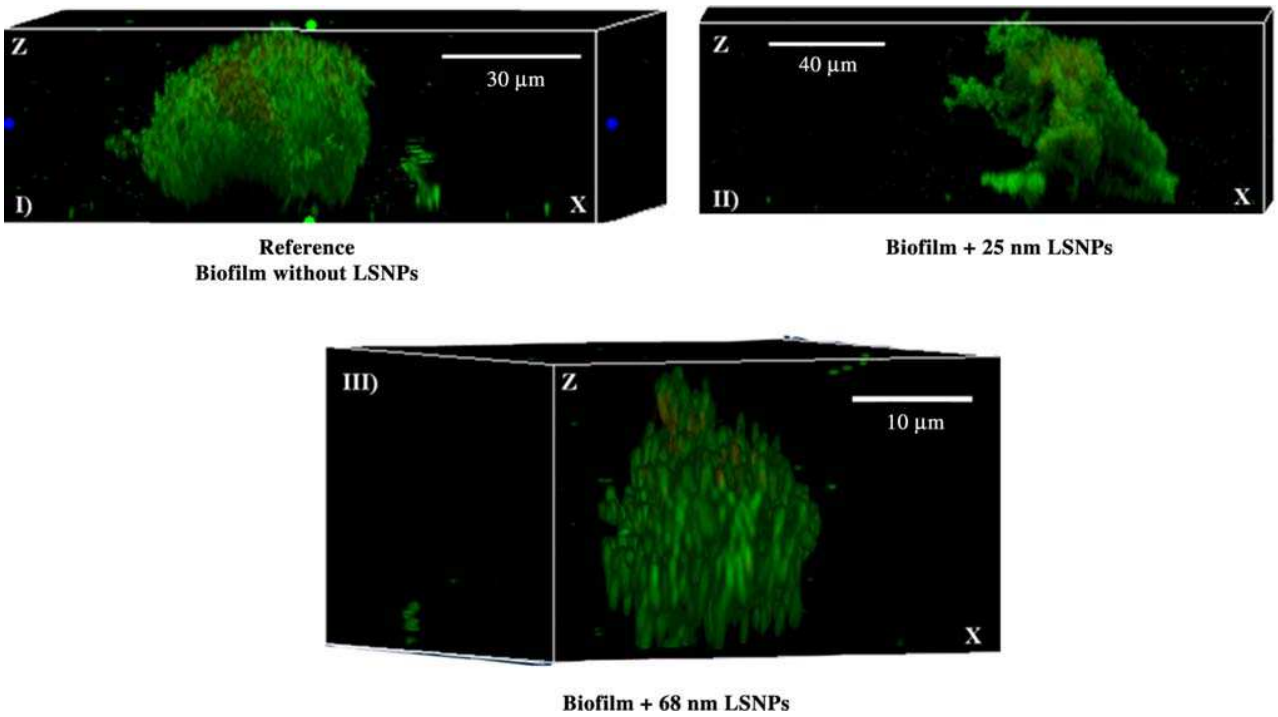

Figure 7. Determination of the toxicity of the LSNPs (0.5 mg cm^{-3}). (I) Biofilm of *P. aeruginosa* PAO1 without LSNPs (reference); (II) with 25 nm particles; and (III) with 68 nm particles. Live bacteria, labeled with SYTO9® appear green ($\lambda_{exc} = 488$ nm; $\lambda_{em} = 498$–533 nm) and damaged bacteria labeled with propidium iodine appear red ($\lambda_{exc} = 543$ nm; $\lambda_{em} = 575$–700 nm).

Spatial distribution of BSNPs through biofilms

In order to visualize bacteria (SYTO45®), EPS (ConA-Alexa Fluor®488) and BSNPs simultaneously, a triple-labeling method, described in the "Materials and methods" section, was chosen to investigate the spatial distribution of BSNPs of different surface properties and sizes in the biofilm.

25 nm BSNPs

Hydrophilic particles *Ru@Si*, *Ru@Si-A*, *Ru@Si-B,* and *Ru@Si-C* were able to penetrate through the biofilm regardless of surface charge. In Figure 8I, the 2D image visualizes simultaneously the luminescence of bacteria and *Ru@Si-C* BSNPs, whereas the 2D image in Figure 8II visualizes only the *Ru@Si-C* BSNPs. Labeling the bacteria in blue (Figure 8I) allows the morphology of the biofilm to be visualized and Figure 8II indicates, in red, the presence of the *Ru@Si-C* over the whole area of the biofilm. This observation was confirmed with the 3-dimensional representation of *Ru@Si-C* (Figure 8III). The same 2-dimensional images were taken using hydrophobic *Ru@Si-D* nanoparticles; the results are shown in Figure 9I–II. The behavior of *Ru@Si-D* differed from that of the hydrophilic nanoparticles; they were observed to aggregate around the biofilm. To evaluate the penetration of the BSNPs through the biofilm, a ROI inside the biofilm was selected to compare the luminescence intensity of different stacks from the bottom to the top of the biofilm. Figure 10 shows the luminescence intensity of the different 25 nm BSNPs as a function of the normalized thickness. As the thicknesses of the biofilms were similar to each other (25–34 µm for the five experiments), it can be argued that the penetration ability of each kind of particle in the different biofilms can be compared directly. For hydrophobic nanoparticles (*Ru@Si-D*), the luminescence intensity differed from zero only in the upper part of the biofilm (0.85–1.0), whereas the luminescence intensity of the hydrophilic particles was observed throughout the entire thickness and was always minimal at the normalized thickness of 1. So in pseudo-static conditions and with a contact time of 16 h, it is proposed that hydrophilic nanoparticles penetrated the whole biofilm whereas the hydrophobic *Ru@Si-D* particles remained at the top and on the edge of the biofilm.

68 nm BSNPs

Figure 11 shows the penetration curves of the 68 nm and 25 nm *Ru@Si-C* (Figure 11I) and *Ru@Si-D* (Figure 11II) BSNPs containing ammonium and trimethylsilyl groups, respectively. For both hydrophobic and hydrophilic BSNPs the images and the penetration curves showed a significant decrease in the intensity with increasing particle size indicating deeper penetration of the smaller hydrophilic particles. The penetration curves of all hydrophilic nanoparticles *Ru@Si*, *Ru@Si-A*, *Ru@Si-B,* and *Ru@Si-C* exhibited a similar behavior (Figure S4). The hydrophobic *Ru@Si-D* particles behaved similarly to each other whatever their size. It is likely that the penetration of *Ru@Si-D* particles through the biofilm was underestimated, nevertheless these particles were clearly visualized at the top (Figure 11II) and at the edge of the biofilm down its entire height (Figure S5).

CLSM observations show that hydrophilic nanoparticles were distributed throughout the whole biofilm, which is not surprising in aggregates of microorganisms composed of up to 90% water (Flemming & Wingender 2010). A transfer limitation was also noted for the particles on the upper part of the biofilm (from 60% of the thickness) even after 16 h of contact, as mentioned by Drury, Characklis et al. (1993) and Drury, Stewart et al. (1993) for mature biofilms of *P. aeruginosa*. In contrast

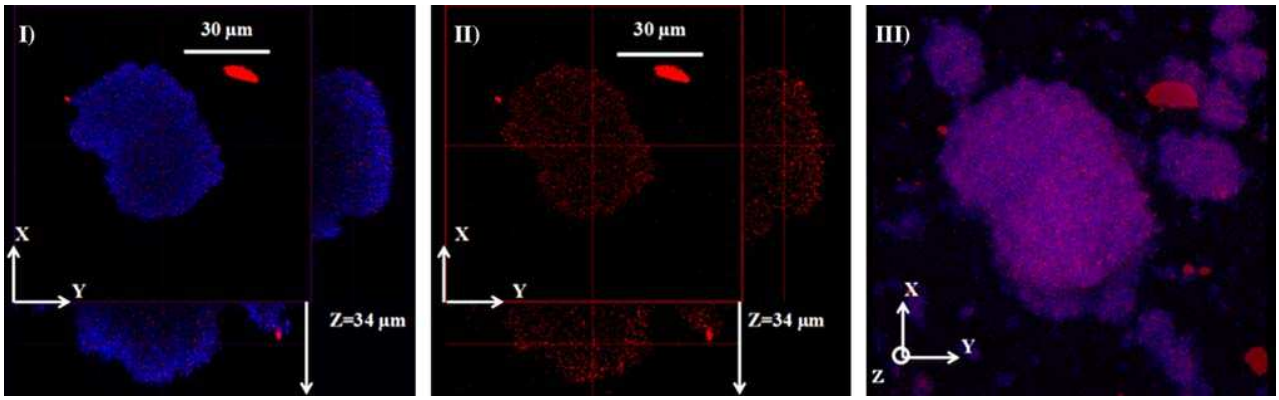

Figure 8. 2D images of *Ru@Si-C* particles in a biofilm of *P. aeruginosa* (I) and (II); 3D image of *Ru@Si-C* particles in a biofilm of *P. aeruginosa* (III). Bacterial DNA is labeled with SYTO45® and appears blue (λ_{exc} = 458 nm; λ_{em} = 468–488 nm) and *Ru@Si-C* particles appear red (λ_{exc} = 543 nm; λ_{em} = 600–700 nm).

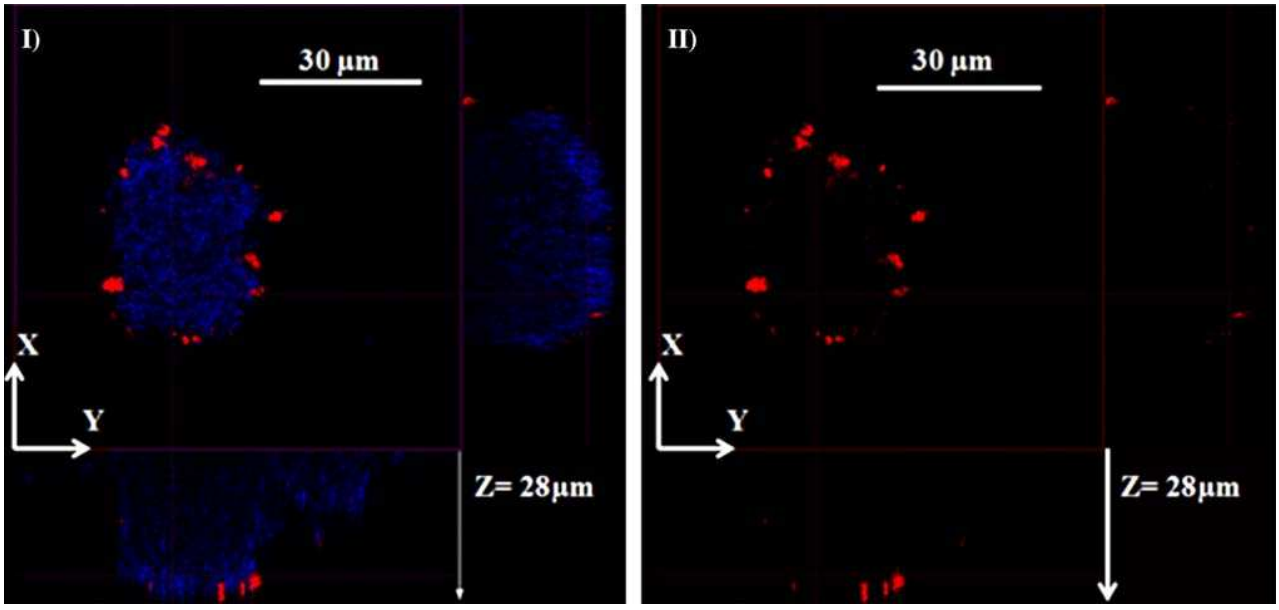

Figure 9. 2D images of *Ru@Si-D* particles in a biofilm of *P. aeruginosa* (I) and (II). Bacterial DNA is labeled with SYTO45® and appears blue (λ_{exc} = 458 nm; λ_{em} = 468–488 nm) and *Ru@Si-D* particles appear red (λ_{exc} = 543 nm; λ_{em} = 600–700 nm).

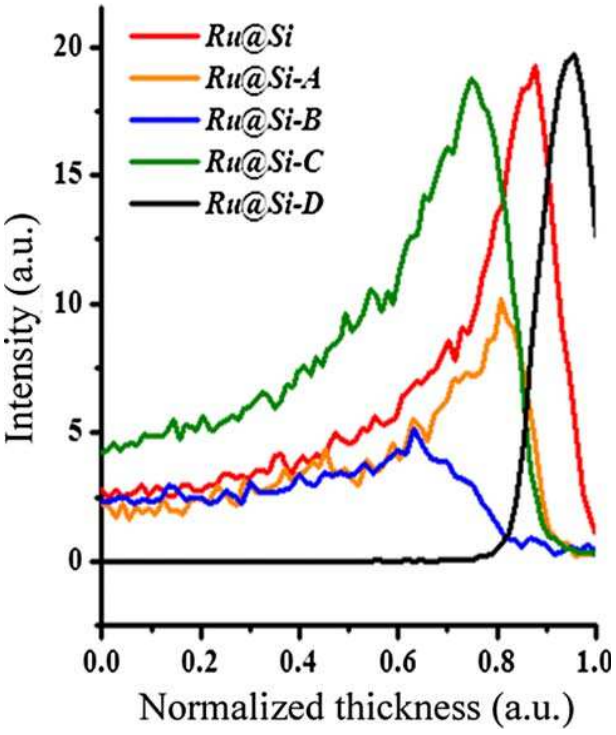

Figure 10. Penetration curves of 25 nm BSNPs. Emission intensity as a function of the normalized thickness of the biofilm.

with hydrophilic particles, hydrophobic particles appeared at the edge of the biofilm of *P. aeruginosa* PAO1, forming some aggregates as shown in Figure 9 without visible penetration of 25 nm *Ru@Si-D* inside the biofilm. This was confirmed by examining the optical sections of biofilm at mid-height, and by comparing the behavior of hydrophilic and hydrophobic BSNPs (Figure S6) since *Ru@Si-D* were localized all around the biofilm (Figure S6IIIa and b) whereas no such crown was observed in the case of hydrophilic *Ru@Si-C* (Figure S6I and IIa and b). If hydrophobic BSNPs were able to penetrate the biofilm they should have been seen in the optical sections. This result is in agreement with Chan et al. (2005) and Kuo et al. (2007) who identified hydrophobic interactions between cationic antimicrobial peptides (having a hydrophobic sequence) and alginates of biofilms of *P. aeruginosa*. Recently, Aldeek et al. (2011) labeled hydrophobic microdomains in biofilms of *Shewanella oneidensis* using hydrophobic QD. These particles concentrated in clusters, suggesting their confinement in a more hydrophobic environment. Turakhia et al. (1983) and more recently Flemming and Wingender (2010) showed that the cohesion and the maintenance of biofilms were facilitated by the presence of hydrophobic microdomains and the cross-linking of divalent cations (Ca^{2+} and Mg^{2+}) which ensured the formation of a stable network.

All hydrophilic nanoparticles (cationic and anionic) penetrated the entire biofilm, but the overall penetration of nanoparticles with a grafted quaternary ammonium, *Ru@Si-C*, (ε = +43 mV) appeared greater although their hydrophilic balance was similar (Figure 10). Hydrophilicity alone cannot explain the difference in behavior of these BSNPs. While physico-chemical interactions could be proposed between BSNPs and the EPS matrix and/or the membrane cells, which are globally negatively

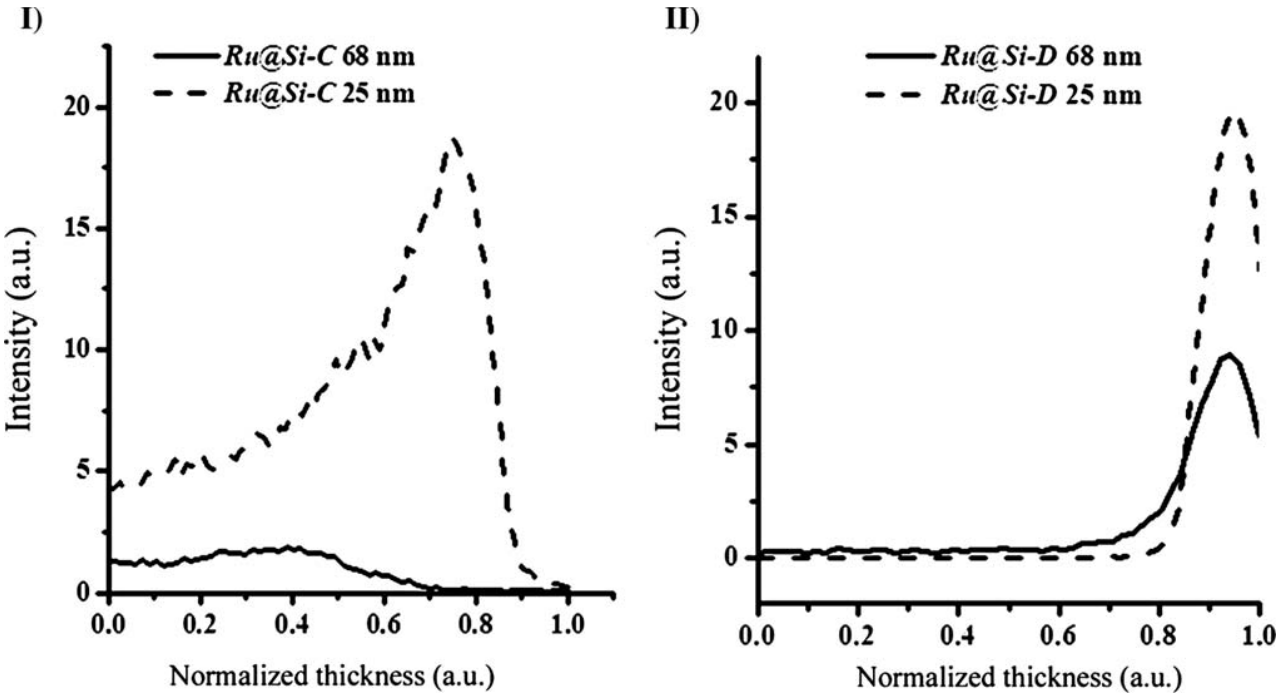

Figure 11. Penetration curves of 68 and 25 nm BSNPs (I) *Ru@Si-C* and (II) *Ru@Si-D*. Emission intensity as a function of the normalized thickness of the biofilm.

charged (May & Chakrabarty 1994; Friedman & Kolter 2004), complementary studies will have to be performed to ascertain the specific nature of the interactions.

Although the quaternary ammonium compounds are known to act as a biocide (Campanac et al. 2002), *Ru@Si-C* particles did not affect the viability or structure of the biofilm even after 16 h of contact, probably due to a very low concentration of the ammonium moiety, less than 5×10^{-8} mol cm^{-3} according to the grafting ratio of these BSNPs.

Finally, a size effect has been highlighted using two nanosized BSNPs. Such behavior could indicate that narrow diffusion paths exist throughout the biofilm.

Conclusions

In this work, luminescent particles were prepared in large quantities and with a controlled size and intense photoluminescence emission. The surfaces of the particles can be chemically modified. These particles were characterized extensively using different techniques (DRIFT, ^{13}C and ^{29}Si solid state NMR, XPS, elementary analysis, photoluminescence, and zeta potential). Before the exploration of biofilms of *P. aeruginosa* PAO1 with BSNPs, a preliminary study showed that LSNPs are not toxic until their mass concentration reached 0.5 mg cm^{-3}. Using CLSM, these novel BSNPs were visualized in a biofilm of *P. aeruginosa* for the first time. The difference in penetration of particles through the biofilm as a function of the size and the surface functionalization was demonstrated, although the exact localization of the silica nanoparticles cannot be ascertained. The present study shows that the hydrophilic particles penetrate throughout the biofilm regardless of the size, but a steric effect was observed, the smaller particles diffusing in greater number than the larger ones. For hydrophobic nanoparticles, an accumulation at the periphery of the biofilm was observed regardless of the particle size. This observation suggests that the functionalization of the particles could be a key factor in the penetration of particles in the biofilm. The effect of size also has to be carefully considered. These results emphasize that BSNPs are powerful and innovative tools for the study of bacterial biofilms. In contrast to latex particles, silica has the advantage of displaying a wide variety of functional surface groups.

Acknowledgments

LM thanks MESR for a grant and Cofecub for its funding in the project with Brazil.

References

Aldeek F, Mustin C, Balan L, Roques-Carmes T, Fontaine-Aupart M-P, Schneider R. 2011. Surface-engineered quantum dots for the labeling of hydrophobic microdomains in bacterial biofilms. Biomaterials. 32:5459–5470.

Brinker C, Scherer G. 1990. Sol-gel science: the physics and chemistry of sol-gel processing. San Diego (CA): Acadamic Press/Elsevier Science.

Brooun A, Liu S, Lewis K. 2000. A dose-response study of antibiotic resistance in *Pseudomonas aeruginosa* biofilms. Antimicrob Agents Chemother. 44:640–646.

Campanac C, Pineau L, Payard A, Baziard-Mouysset G, Roques C. 2002. Interactions between biocide cationic agents and bacterial biofilms. Antimicrob Agents Chemother. 46:1469–1474.

Chan C, Burrows LL, Deber CM. 2005. Alginate as an auxiliary bacterial membrane: binding of membrane-active peptides by polysaccharides. J Pept Res. 65:343–351.

Costerton JW, Lewandowski Z, Caldwell DE, Korber DR, Lappin-Scott HM. 1995. Microbial biofims. Ann Rev Microbiol. 49:711–745.

Cousinie S, Gressier M, Alphonse P, Menu M-J. 2007. Silica-based nanohybrids containing dipyridine, urethan, or urea derivatives. Chem Mater. 19:6492–6503.

Cousinie S, Mauline L, Gressier M, Kandibanda SR, Datas L, Reber C, Menu M-J. 2012. Bulk or surface grafted silylated Ru(II) complexes on silica as luminescent nanomaterials. New J Chem. 36:1355–1367.

de Beer D, Stoodley P, Roe F, Lewandowski Z. 1994. Effects of biofilm structures on oxygen distribution and mass transport. Biotechnol Bioeng. 43:1131–1138.

de Beer D, Stoodley P, Lewandowski Z. 1994. Liquid flow in heterogeneous biofilms. Biotechnol Bioeng. 44:636–641.

Doggett RG, Harrison GM, Stillwell RN, Wallis ES. 1966. An atypical *Pseudomonas aeruginosa* associated with cystic fibrosis of the pancreas. J Pediatr. 68:215–221.

Drury WJ, Characklis WG, Stewart PS. 1993. Interactions of 1 μm latex particles with *Pseudomonas aeruginosa* biofilms. Water Res. 27:1119–1126.

Drury WJ, Stewart PS, Characklis WG. 1993. Transport of 1-μm latex particles in *Pseudomonas aeruginosa* biofilms. Biotechnol Bioeng. 42:111–117.

Flemming H-C, Wingender J. 2010. The biofilm matrix. Nat Rev Micro. 8:623–633.

Forier K, Messiaen AS, Raemdonck K, Deschout H, Rejman J, De Baets F, Nelis H, De Smedt SC, Demeester J, Coenye T, Braeckmans K. 2012. Transport of nanoparticles in cystic fibrosis sputum and bacterial biofilms by single-particle tracking microscopy. Nanomedecine. 1–15. doi: 10.2217/nnm.12.129

Friedman L, Kolter R. 2004. Two genetic loci produce distinct carbohydrate-rich structural components of the *Pseudomonas aeruginosa* biofilm matrix. J Bacteriol. 186:4457–4465.

Guiot E, Georges P, Brun A, Fontaine-Aupart MP, Bellon-Fontaine MN, Briandet R. 2002. Heterogeneity of diffusion inside microbial biofilms determined by fluorescence correlation spectroscopy under two-photon excitation. Photochem Photobiol. 75:570–578.

Habimana O, Steenkeste K, Fontaine-Aupart M-P, Bellon-Fontaine M-N, Kulakauskas S, Briandet R. 2011. Diffusion of nanoparticles in biofilms is altered by bacterial cell wall hydrophobicity. Appl Environ Microbiol. 77:367–368.

Hall-Stoodley L, Stoodley P. 2005. Biofilm formation and dispersal and the transmission of human pathogens. Trends Microbiol. 13:7–10.

Herr JK, Smith JE, Medley CD, Shangguan D, Tan W. 2006. Aptamer-conjugated nanoparticles for selective collection and detection of cancer cells. Anal Chem. 78:2918–2924.

Hidalgo G, Burns A, Herz E, Hay AG, Houston PL, Wiesner U, Lion LW. 2009. Functional tomographic fluorescence imaging of pH microenvironments in microbial biofilms by use of silica nanoparticle sensors. Appl Environ Microbiol. 75:7426–7435.

Huq A, Whitehouse CA, Grim CJ, Alam M, Colwell RR. 2008. Biofilms in water, its role and impact in human disease transmission. Curr Opin Biotechnol. 19:244–247.

Jiang H, Wang G, Zhang W, Liu X, Ye Z, Jin D, Yuan J, Liu Z. 2010. Preparation and time-resolved luminescence bioassay Application of multicolor luminescent lanthanide nanoparticles. J Fluoresc. 20:321–328.

Jin Y, Lohstreter S, Pierce DT, Parisien J, Wu M, Hall C, Zhao JX. 2008. Silica nanoparticles with continuously tunable sizes: synthesis and size effects on cellular contrast imaging. Chem Mater. 20:4411–4419.

Khalilzadeh P, Lajoie B, El Hage S, Furiga A, Baziard G, Berge M, Roques C. 2010. Growth inhibition of adherent *Pseudomonas aeruginosa* by an *N*-butanoyl-l-homoserine lactone analog. Can J Microbiol. 56:317–325.

Kim JS, Yoon T-J, Yu KN, Kim BG, Park SJ, Kim HW, Lee KH, Park SB, Lee JK, Cho MH. 2006. Toxicity and tissue distribution of magnetic nanoparticles in mice. Toxicol Sci. 89:338–347.

Kumar R, Roy I, Ohulchanskyy TY, Goswami LN, Bonoiu AC, Bergey EJ, Tramposch KM, Maitra A, Prasad PN. 2008. Covalently dye-linked, surface-controlled, and bioconjugated organically modified silica nanoparticles as targeted probes for optical imaging. ACS Nano. 2:449–456.

Kuo HH, Chan C, Burrows LL, Deber CM. 2007. Hydrophobic interactions in complexes of antimicrobial peptides with bacterial polysaccharides. Chem Biol Drug Des. 69:405–412.

Lau PCY, Lindhout T, Beveridge TJ, Dutcher JR, Lam JS. 2009. Differential lipopolysaccharide core capping leads to quantitative and correlated modifications of mechanical and structural properties in *Pseudomonas aeruginosa* biofilms. J Bacteriol. 191:6618–6631.

Lawrence JR, Korber DR, Hoyle BD, Costerton JW, Caldwell DE. 1991. Optical sectioning of microbial biofilms. J Bacteriol. 173:6558–6567.

Lian W, Litherland SA, Badrane H, Tan W, Wu D, Baker HV, Gulig PA, Lim DV, Jin S. 2004. Ultrasensitive detection of biomolecules with fluorescent dye-doped nanoparticles. Anal Biochem. 334:135–144.

Little BJ, Lee JS, Ray RI. 2008. The influence of marine biofilms on corrosion: a concise review. Electrochim Acta. 54:2–7.

Liu S, Han M. 2005. Synthesis, functionalization, and bioconjugation of monodisperse, silica-coated gold nanoparticles: robust bioprobes. Adv Funct Mater. 15:961–967.

Lytle FE, Hercules DM. 1969. Luminescence of tris(2,2′-bipyridine)ruthenium(II) dichloride. J Am Chem Soc. 91:253–257.

Maciel GE, Sindorf DW. 1980. Silicon-^{29} NMR study of the surface of silica gel by cross polarization and magic-angle spinning. J Am Chem Soc. 102:7606–7607.

Mah T-FC, O'Toole GA. 2001. Mechanisms of biofilm resistance to antimicrobial agents. Trends Microbiol. 9: 34–39.

May TB, Chakrabarty AM. 1994. Isolation and assay of *Pseudomonas aeruginosa* alginate. Methods Enzymol. 235:295–304.

Morrow JB, Arango CP, Holbrook RD. 2010. Association of quantum dot nanoparticles with *Pseudomonas aeruginosa* biofilm. J. Environ Qual. 39:1934–1941.

Moulder JF, Stickle WF, Sobol PE, Bomben KD. 1992. Handbook of X-ray photoelectron spectroscopy. Eden Prairie (MN): Physical Electronics/Perkin Elmer.

Okabe S, Yasuda T, Watanabe Y. 1997. Uptake and release of inert fluorescence particles by mixed population biofilms. Biotechnol Bioeng. 53:459–469.

Qian J, Zhang C, Cao X, Liu S. 2010. Versatile immunosensor using a quantum dot coated silica nanosphere as a label for signal amplification. Anal Chem. 82:6422–6429.

Santra S, Zhang P, Wang K, Tapec R, Tan W. 2001. Conjugation of biomolecules with luminophore-doped silica nanoparticles for photostable biomarkers. Anal Chem. 73:4988–4993.

Shi B, Wang Y, Guo Y, Wang Y, Wang Y, Guo Y, Zhang Z, Liu X, Lu G. 2009. Aminopropyl-functionalized silicas synthesized by W/O microemulsion for immobilization of penicillin G acylase. Catal Today. 148:184–188.

Sindorf DW, Maciel GE. 1981. Silicon-^{29} CP/MAS NMR studies of methylchlorosilane reactions on silica gel. J Am Chem Soc. 103:4263–4265.

Sindorf DW, Maciel GE. 1983. Silicon-^{29} NMR study of dehydrated/rehydrated silica gel using cross polarization and magic-angle spinning. J Am Chem Soc. 105:1487–1493.

Singh R, Paul D, Jain RK. 2006. Biofilms: implications in bioremediation. Trends Microbiol. 14:389–397.

Stoodley P, deBeer D, Lewandowski Z. 1994. Liquid flow in biofilm systems. Appl Environ Microbiol. 60:2711–2716.

Sutra P, Fajula F, Brunel D, Lentz P, Daelen G, Nagy JB. 1999. ^{29}Si and ^{13}C MAS-NMR characterization of surface modification of micelle-templated silicas during the grafting of organic moieties and end-capping. Colloids Surf A. 158:21–27.

Tripathi S, Champagne D, Tufenkji N. 2012. Transport behavior of selected nanoparticles with different surface coatings in granular porous media coated with *Pseudomonas aeruginosa* biofilm. Environ Sci Technol. 46:6942–6949.

Turakhia MH, Cooksey KE, Characklis WG. 1983. Influence of a calcium-specific chelant on biofilm removal. Appl Environ Microbiol. 46:1236–1238.

Voisin P, Ribot EJ, Miraux S, Bouzier-Sore AK, Lahitte JF, Bouchaud V, Mornet S, Thiaudière E, Franconi JM, Raison L, et al. 2007. Use of lanthanide-grafted inorganic nanoparticles as effective contrast agents for cellular uptake imaging. Bioconjugate Chem. 18:1053–1063.

Wahl M, Goecke F, Labes A, Dobretsov S, Weinberger F. 2012. The second skin: ecological role of epibiotic biofilms on marine organisms. Front Microbiol. 3:1–21, doi: 10.3389/fmicb.2012.00292.

Wang Z, Miu T, Xu H, Duan N, Ding X, Li S. 2010. Sensitive immunoassay of *Listeria monocytogenes* with highly fluorescent bioconjugated silica nanoparticles probe. J Microbiol Methods. 83:179–184.

Wang Z, Xu H, Wu J, Ye J, Yang Z. 2011. Sensitive detection of Salmonella with fluorescent bioconjugated nanoparticles probe. Food Chem. 125:779–784.

White DG, McDermott PF. 2001. Biocides, drug resistance and microbial evolution. Curr Opin Microbiol. 4:313–317.

Wingender J, Neu TR, Flemming H-C. (Eds.). 1999. Microbial extracellular polymeric substances: characterization, structure and function. Berlin: Springer. Chapter 1, What are bacterial extracellular polymeric substances? Berlin (Germany): Springer; p. 1–15.

Yang H-H, Qu H-Y, Lin P, Li S-H, Ding M-T, Xu J-G. 2003. Nanometer fluorescent hybrid silica particle as ultrasensitive and photostable biological labels. Analyst. 128:462–466.

Yang Y, Yan X, Cui Y, He Q, Li D, Wang A, Fei J, Li J. 2008. Preparation of polymer-coated mesoporous silica nanoparticles used for cellular imaging by a “graft-from” method. J Mater Chem. 18:5731–5737.

Zhao X, Hilliard LR, Mechery SJ, Wang Y, Bagwe RP, Jin S, Tan W. 2004. A rapid bioassay for single bacterial cell quantitation using bioconjugated nanoparticles. Proc Natl Acad Sci USA. 101:15027–15032.